SCIENCE CHINA
Information Sciences

• RESEARCH PAPER •
Special Focus on Space Flexible Manipulation and Control for On-orbit Servicing

May 2017, Vol. 60 050203:1–050203:15
doi: 10.1007/s11432-016-9035-0

Vibration suppression of a large flexible spacecraft for on-orbit operation

Deshan MENG[1,2,3], Houde LIU[3], Yanan LI[3], Wenfu XU[1*] & Bin LIANG[1,3*]

[1] *Shenzhen Graduate School, Harbin Institute of Technology, Shenzhen* 518055, *China;*
[2] *Department of Mechanical and Aerospace Engineering, The Ohio State University, Columbus* 43210, *USA;*
[3] *Shenzhen Key Lab of Space Robotic Technology and Telescience, Shenzhen Graduate School, Tsinghua University, Shenzhen* 518055, *China*

Received December 13, 2016; accepted January 17, 2017; published online April 1, 2017

Abstract Flexible appendages, such as solar panels, communication antennas and other large structures, are mounted on the base of a space robot and target satellite. The vibration of the flexible structure is excited by operations of a space manipulator. It is very challenging to control the vibration of large flexible appendages for on-orbit operation and, especially when the manipulator operates a non-cooperative target with unknown structural parameters and vibration information. In this study, a hybrid control method is proposed based on wave-based control and PD control methods to control the motion of a manipulator while suppressing the vibration of appendages. First, the rigid-flexible coupled dynamic model of a compounded system is established. This is followed by designing a hybrid control strategy combining wave-based control and PD control for rest-to-rest maneuvers based on the characteristics of the compounded system. Finally, the simulation of a 3D compounded system is provided to verify the effectiveness of the presented approach. The simulation results indicate that the space robot can successfully berth the target while suppressing the vibrations of the structure.

Keywords space robot, large flexible spacecraft, vibration suppression, wave-based control, on-orbit operation

Citation Meng D S, Liu H D, Li Y N, et al. Vibration suppression of a large flexible spacecraft for on-orbit operation. Sci China Inf Sci, 2017, 60(5): 050203, doi: 10.1007/s11432-016-9035-0

1 Introduction

Robotic systems are expected to play an increasingly important role in future space activities such as repairing, upgrading, refueling, and re-orbiting spacecraft [1–4]. As a service object, a spacecraft such as a GEO satellite for broadcasting, communication, and weather forecasts, is growing in size to satisfy increasingly demanding mission requirements. Large flexible components, such as antenna reflectors and solar paddles, are inevitably mounted on the spacecraft. For example, the Japanese Engineering Test Satellite VIII (ETS-VIII) has a size of 40 m × 37 m and a mass of 3000 kg [5]. Two large deployable reflectors are appended in the roll axis direction, and a pair of solar paddles rotates around the pitch axis at a rate of 360°/day to continuously face the sun. The modeling of a large flexible spacecraft on orbit

* Corresponding author (email: wfxu@hit.edu.cn, bliang@mail.tsinghua.edu.cn)

is a complex task [6]. Conversely, a space robot used to complete on-orbit servicing tasks also has generally flexible solar panels. It is very challenging for this type of a space robot to capture and repair large flexible satellites.

Recently, researchers focused on studying space robots with flexible appendages to capture and manipulate large flexible satellites. Gasbarri and Pisculli [7] proposed a mixed Newton-Euler/Euler-Lagrange modeling formulation for a space robot and a spacecraft with flexible solar arrays. This was followed by two control strategies involving compensation of the flexibility excitation of the chaser satellite solar panels during the capture of a flexible target spacecraft that were presented and applied to a grasping maneuver. The spatial dynamics and control of a 6-DOF space robot with flexible panels was examined in a previous study [8]. The computed torque control method was used to design an active controller to suppress spacecraft drift caused by impact. Zarafshan et al. [9] derived the dynamics model by virtually partitioning the entire system into rigid and flexible portions, and developed an adaptive hybrid suppression control algorithm. Hirano et al. [10, 11] developed a simple dynamic model of space robot with a rigid manipulator and a flexible appendage, which was modeled using a virtual joint model. Kojima and Kasai [12, 13] applied the input-shaping technique to control the link motion of a planar space robot that was equipped with a single flexible appendage. Azadi et al. [14] studied the vibration suppression of a smart flexible satellite moving in a circular orbit by using piezoelectric layers as sensors and actuators. In [15] an adaptive-robust control scheme was used to achieve the large angle trajectory tracking of a satellite and suppress the vibration of the appendages. Xu et al. [16] developed a dynamic model and a closed-loop simulation system of a space robot with two flexible appendages to capture a large flexible spacecraft. A few planning and control strategies for reducing the residual vibration were also presented based on the dynamic simulation and analysis of different cases.

It is very challenging to control the vibration of large flexible non-cooperative satellites when these satellites are manipulated by a space robot. This is due to the following reasons: First, it is difficult to identify the mass inertia parameters of non-cooperative spacecrafts are difficult. Specifically, it is difficult to accurately identify the structural vibration parameters of flexible appendages. Second, it is not easy to measure the vibration information of flexible appendages. Thus, due to the fore-mentioned constraints, it is difficult to practically perform control methods that require vibration information related to a flexible appendages as the feedback signal or require an the accurate model. Over the last few years, a vibration control method based on wave-echo principle was studied in the control of lumped flexible systems. O'Connor [17, 18] firstly applied the wave-based control method in a lumped-parameter mass-spring system. Cleary et al. [19] applied the wave-based method to control space debris motion via an elastic tether. The use of the wave-based method can achieve an arbitrary change in the target with respect to the magnitude and direction of its velocity while ensuring the control of the tether and debris. Marek [20] researched the implementation of wave-based control for experiments using a servomotor. In [21], the wave-based method was used for oscillation damping of elastic-link robotic arms, and a practical application of the oscillation damping on a multi-elastic-link experimental setup was demonstrated. Ref. [22] discussed the vibration suppression of a lumped torsional system using a wave-absorption filter that considered the boundary condition. The main advantage of the wave-based control is that it does not require a precise model of the controlled object. A wave-based method can achieve a significant effect of vibration control by only using the information of the interface between the actuator and the flexible system. The present study focuses on combining the wave-based method and PD control to suppress the vibration of large flexible appendages.

The remainder of this paper is organized as follows. Section 2 establishes the dynamic equations of a compounded system composed of a space robot and a target spacecraft. In Section 3, a hybrid control strategy combining wave-based control and PD control is constructed to suppress the structure vibration. Section 4 presents simulation studies of a typical case by a 7-DOF 3D space robot with a flexible appendage and a target with a large flexible appendage. The final section summarizes and concludes the paper.

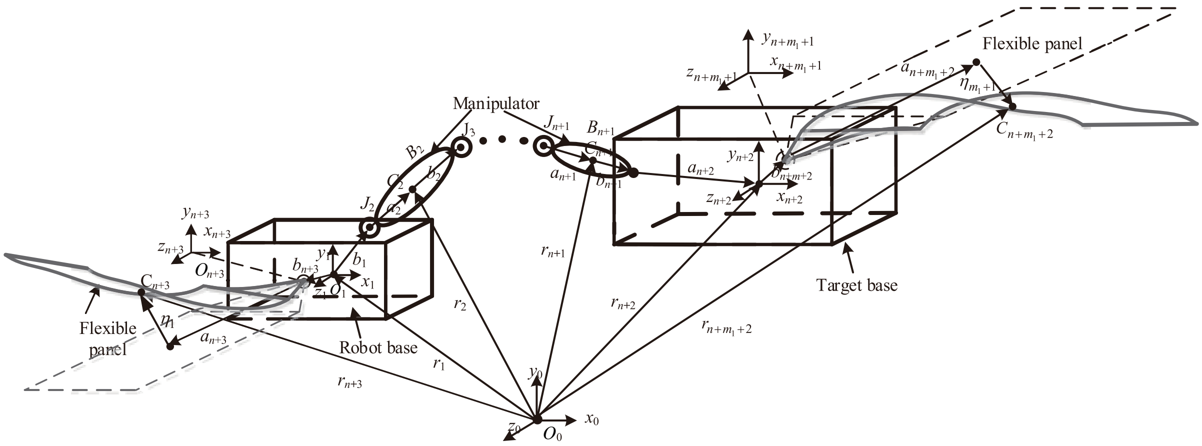

Figure 1 The model of the compounded system.

2 Dynamic modeling of the compounded system

Following capture, a target satellite is locked to the end-effector of a space robotic system with flexible appendages as shown in Figure 1. This is followed by the formation of a new system termed as the compounded system. It is composed of a robot base with m_1 flexible appendages, a serial manipulator (called space manipulator) with n degrees of freedoms (n DOFs), and a target base with m_2 flexible appendages. Each flexible appendage is fixed to a robot base or target base through a fixed hinge. The target base is fixed to the end-effector of the space manipulator through a fixed hinge. Hence, the compounded system can be described by $n{+}m{+}3$ bodies (including the inertial frame) and $n{+}m{+}2$ hinges, $m = m_1 + m_2$.

2.1 Dynamic modeling of the compounded system with flexible appendages

In order to derive the dynamic equations, the symbols (shown in Figure 1) of the compounded system with flexible appendages are defined. Specifically, $\sum_0$ denotes the inertia frame; $\sum_i$ $(i = 1, \ldots, n + 2)$ denotes the body fixed frame of the rigid body B_i; $\sum_i$ $(i = n + 3, \ldots, n + m + 2)$ denotes the floating frame of the flexible body B_i; C_i $(i = 1, \ldots, n + 2)$ denotes the position of the rigid body B_i's CM (center of mass); C_i $(i = n + 3, \ldots, n + m + 2)$ denotes the position of the flexible body B_i's CM; and $r_i \in \mathbb{R}^3$ $(i = 1, \ldots, n + m + 2)$ denotes the position vector of C_i. Additionally, $a_i \in \mathbb{R}^3$ $(i = 2, \ldots, n + 2)$ denotes the position vector from H_{i-1} to C_i; $b_i \in \mathbb{R}^3$ $(i = 1, \ldots, n + 1)$ denotes the position vector from C_i to H_i; $b_i \in \mathbb{R}^3$ $(i = n + 3, \ldots, n + m_1 + 2)$ denotes the position vector from C_1 to H_i; and $b_i \in \mathbb{R}^3$ $(i = n + m_1 + 2, \ldots, n + m + 2)$ denotes the position vector from C_{n+2} to H_i. Furthermore, $\Theta \in \mathbb{R}^n$ is the manipulator motor angle vector, i.e., $\Theta = [\theta_2, \ldots, \theta_{n+1}]^{\mathrm{T}}$; $q \in \mathbb{R}^n$ denotes the manipulator link angle vector; $\varphi \in \mathbb{R}^m$ denotes the elastic variable vector of the flexible appendages; $x_b \in \mathbb{R}^6$ denotes the position and orientation vector of space robot base; and $\Psi_1 \in \mathbb{R}^3$ denotes the base attitude represented by xyz Euler angles.

In this study, the virtual torsion spring and lumped mass are used to approximately describe the flexible solar paddle. As shown in Figure 2, point C denotes the center of mass of the solar paddle. Point B denotes the position at which the solar paddle is connected to the satellite base. Two virtual torsion springs are built at the root of each paddle based on the vibration characteristics of solar paddles. A virtual torsion spring is used to describe the bending vibration, and the other torsion spring is used to describe the torsional vibration.

The dynamic equation of the compounded system with flexible appendages is as follows:

$$\begin{bmatrix} H_{bb} & H_{bq} & H_{b\varphi} \\ H_{bq}^{\mathrm{T}} & H_{qq} & H_{q\varphi} \\ H_{b\varphi}^{\mathrm{T}} & H_{q\varphi}^{\mathrm{T}} & H_{\varphi\varphi} \end{bmatrix} \begin{bmatrix} \ddot{x}_b \\ \ddot{q} \\ \ddot{\varphi} \end{bmatrix} + C\left(x_b, q, \varphi, \dot{x}_b, \dot{q}, \dot{\varphi}\right) \begin{bmatrix} \dot{x}_b \\ \dot{q} \\ \dot{\varphi} \end{bmatrix} + \begin{bmatrix} 0 & & \\ & 0 & \\ & & K_{\varphi} \end{bmatrix} \begin{bmatrix} x_b \\ q \\ \varphi \end{bmatrix} = \begin{bmatrix} 0 \\ \tau_m \\ 0 \end{bmatrix}, \tag{1}$$

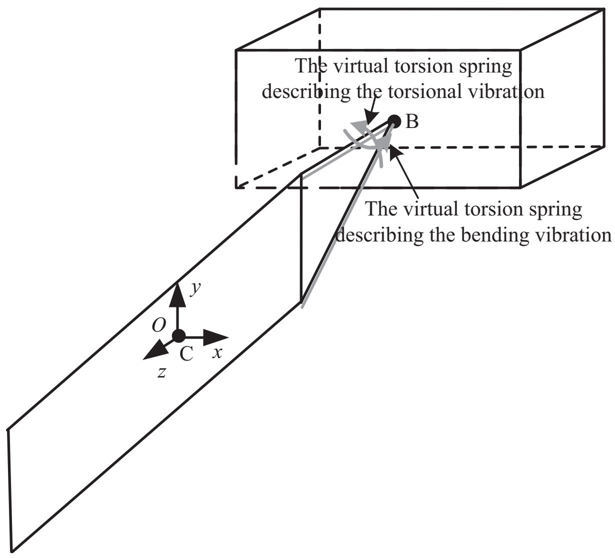

Figure 2 The lumped mass model of the flexible solar paddle.

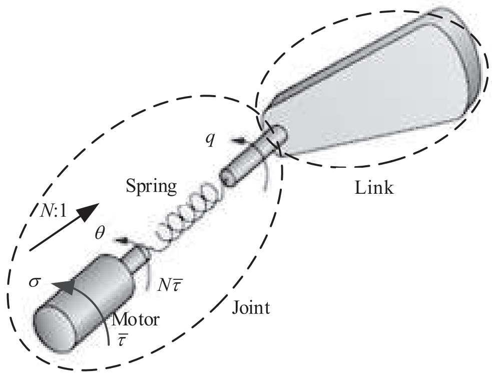

Figure 3 The simplified model of the flexible joint.

where $y = [x_b^{\mathrm{T}}, q^{\mathrm{T}}, \varphi^{\mathrm{T}}]^{\mathrm{T}}$. H_{bb}, H_{bq}, $H_{b\varphi}$, H_{qq}, $H_{q\varphi}$ and $H_{\varphi\varphi}$ denote sub-mass matrices. $C\left(x_b, q, \varphi, \dot{x}_b, \dot{q}, \dot{\varphi}\right)$ denotes the coupling matrix including Coriolis force and centrifugal force. Additionally, K_φ denotes the stiffness matrix of the flexible appendages, and τ_m denotes the manipulator joint torque vector.

2.2 Dynamic modeling of the compounded system with flexible appendages and flexible joints

The flexibility of the manipulator joint is not considered in (1). The simplified model of a flexible joint is shown in Figure 3. Additionally, $\bar{\tau}$ and σ denote the torque and the rotation angle of the motor, respectively. The motor angle is reduced to $\theta\,(=\sigma/N)$ through the harmonic gear reducer, and the output torque is enlarged to $N\bar{\tau}$.

The flexible joint can be simplified as a linear torsion spring unit as shown in Figure 3. The dynamic equation of joint i is as follows [23]:

$$I_i N_i^2 \ddot{\theta}_i + \tau_{mi} = \tau_{si}, \tag{2}$$

where I_i denotes moment of inertia of the motor. τ_{si} denotes the driving torque of joint motor i (the torque output by the gear reducer) and $\tau_{si} = N\bar{\tau}$. τ_{mi} denotes the joint torque caused by spring unit and the following expression:

$$\tau_{mi} = K_{Ji}\left(\theta_i - q_i\right), \tag{3}$$

where K_{Ji} denotes the stiffness of joint i. Combining (1) and (2), the dynamic equation of the compounded

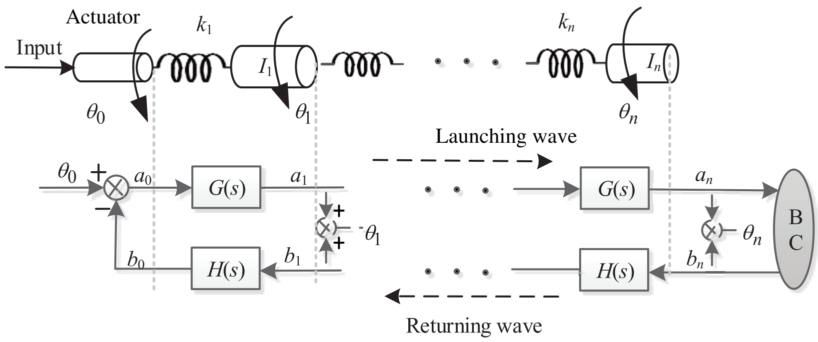

Figure 4 A schematic of the wave-based control.

system with flexible appendages and flexible joints can be obtained as follows:

$$\begin{cases} H\left(y\right)\ddot{y}+C\left(y,\dot{y}\right)\dot{y}+Ky=\tau, \\ J\ddot{\theta}+\tau_m=\tau_s, \end{cases} \tag{4}$$

where $H\left(y\right)$ denotes the mass matrix, $H\left(y\right)=\left[\begin{smallmatrix} H_{bb} & H_{bq} & H_{b\varphi} \\ H_{bq}^{\mathrm{T}} & H_{qq} & H_{q\varphi} \\ H_{b\varphi}^{\mathrm{T}} & H_{q\varphi}^{\mathrm{T}} & H_{\varphi\varphi} \end{smallmatrix}\right]$. K denotes the stiffness matrix, $K=\left[\begin{smallmatrix} 0 & & \\ & 0 & \\ & & K_{\varphi} \end{smallmatrix}\right]$. $\tau=\left[0,\tau_m^{\mathrm{T}},0\right]^{\mathrm{T}}\in\mathbb{R}^n$. $\tau_s=\left[\tau_{s1},\ldots,\tau_{sn}\right]^{\mathrm{T}}\in\mathbb{R}^n$ is a vector composed of driving torques of joint motors; and $\tau_m=\left[\tau_{m1},\ldots,\tau_{mn}\right]^{\mathrm{T}}\in\mathbb{R}^n$ is a vector composed of joint torques. Additionally, $J=\left[\begin{smallmatrix} I_1N_1^2 & & \\ & \ddots & \\ & & I_{n+m}N_{n+m}^2 \end{smallmatrix}\right]\in\mathbb{R}^{n\times n}$ is a diagonal matrix composed of the equivalent moment of inertia of the motor after deceleration.

3 Hybrid control strategy for the vibration suppression of the compounded system during an on-orbit operation

With respect to the compounded system with flexible appendages and flexible joints, the vibration energy is transferred between appendages and the joints of the manipulator. Thus, the vibration information of flexible appendages can be obtained by measuring the deformation or torque of the joints. In this study, a control method combining wave-based control and PD control is designed to solve the vibration suppression for on-orbit operation of large flexible spacecrafts. The suppression of the vibration of large flexible appendages only requires the deformation or torque of manipulator joints. Thus, this method could be potentially used in several engineering applications.

3.1 The wave-based control principle of lumped flexible systems

Wave-based control (WBC) was initially applied to continuous flexible system control. In 1998, O'Connor et al. [17] firstly applied the wave-based control to a lumped flexible system. Wave-based control is a breakthrough control method that can implement control of the flexible system without complete knowledge of the system model. As shown in Figure 4, the core idea of this method involves considering the flexible motion as a superposition of wave motions in two opposite directions [24], and this is termed as: the launching wave and the returning wave. The motion of the actuator is considered as a mechanical wave (launching wave) with respect to the system. The flexibility of the system allows the wave to propagate in the system and returns after a certain boundary condition. The vibration of the flexible system can be effectively suppressed if the return wave is absorbed. Specifically, $G(s)$ and $H(s)$ denote the wave transfer functions.

With respect to a system with infinite extension at one end, the wave enters the system to spread to the right without reflection. This type of flexible system does not generate vibration. The wave-based

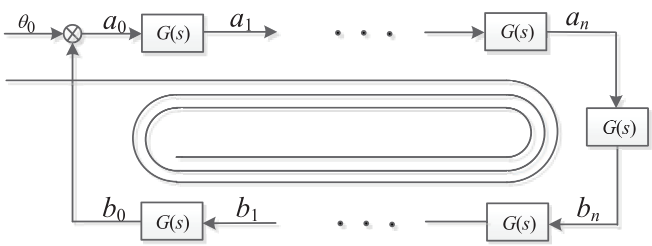

Figure 5 Infinite loop of the wave.

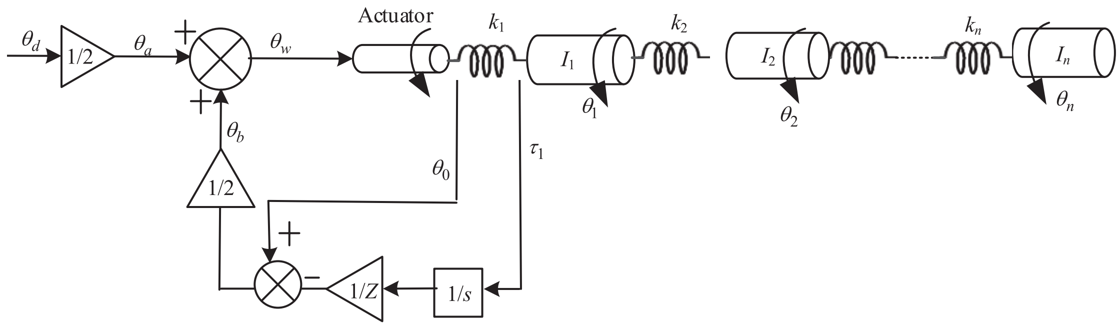

Figure 6 The model of wave-based control for rotating the lumped flexible system.

method adopts this principle to eliminate vibration. With respect to a flexible system, there is no return wave if it is assumed that there is another actuator that absorbs the launching wave at the right end. However, most actual systems only involve a single actuator. Therefore, only the same actuator can be used to complete the wave emission and absorption. As shown in Figure 5, the actuator launches the wave that is reflected at the free end into the system, and the returning wave is finally absorbed by the same actuator. This loop process is equivalent to an infinite extension of the system.

It is necessary to satisfy three conditions to imitate the circulation of the wave. First, the wave can propagate through the system. Second, the wave can be completely reflected at the free end. Finally, the reflected wave can be completely absorbed. If the boundary is free and the wave transfer function $G(s) = H(s)$, then the launching wave can be completely reflected at the right boundary, and the boundary condition satisfies $b_n = a_n G(s)$ as demonstrated in [18].

A simple and effective waveform control scheme is shown in Figure 6. The input of the actuator consists of the following two parts:

$$\theta_w(t) = \theta_a(t) + \theta_b(t), \tag{5}$$

where $\theta_a(t)$ denotes the launch displacement and its value corresponds to half of the desired value $\theta_d(t)$ as detailed in the following expression:

$$\theta_a(t) = \frac{1}{2}\theta_{\mathrm{d}}(t). \tag{6}$$

In (5), $\theta_b(t)$ denotes return displacement. The calculation of return displacement is very important because it is related to the effect of vibration absorption. Several methods exist to calculate return displacement [25]. In this study, the force impedance method that is suitable for a complex system is adopted. Furthermore, θ_b is calculated as follows:

$$\theta_b(t) = \frac{1}{2}\left[\theta_0(t) - \frac{1}{Z}\int \tau_0(t)\,\mathrm{d}t\right] = \frac{1}{2}\left[\theta_0(t) - \omega_n \int [\theta_0(t) - \theta_1(t)]\,\mathrm{d}t\right], \tag{7}$$

where τ_0 denotes the torque of the flexible joint torsion spring that is directly associated with the actuator and $\tau_0 = k_1(\theta_0 - \theta_1)$. Additionally, Z denotes the impedance coefficient and can be defined as $Z = \lambda\sqrt{k_1 I_1}$, and λ denotes a coefficient with a value greater than zero and $\omega_n = \frac{1}{\lambda}\sqrt{\frac{k_1}{I_1}}$. As observed from (7), θ_b is composed of two parts in which the first part implements the other half of the desired input and the

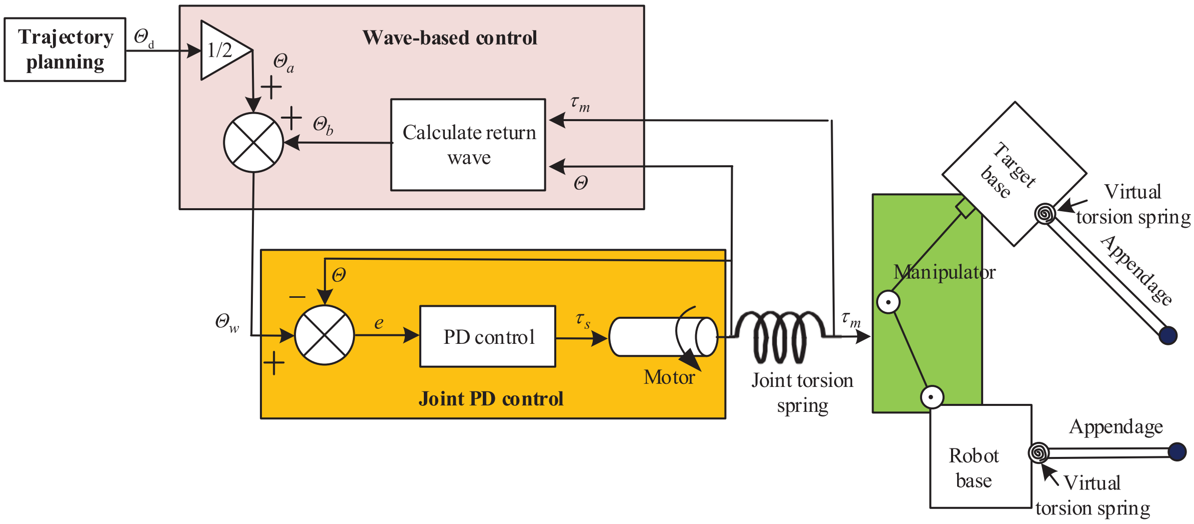

Figure 7 (Color online) Hybrid control strategy for a large flexible spacecraft in-orbit operation.

second part is related to the return torque of the first flexible joint. The introduction of the force integral term in θ_b has two effects, namely an effect in which the vibration of the system is absorbed and an other effect that ensures the final position of θ_0, which is equal to the final value of the desired input θ_d for rest-to rest maneuvers.

It is assumed that the actuator can exactly track the reference input, and thus the following equation holds

$$\theta_0(t) = \theta_w(t). \tag{8}$$

Substituting (5)–(7) into (8), the following equation is obtained

$$\theta_0(t) = \theta_\mathrm{d}(t) - \frac{1}{Z}\int \tau_0(t)\,\mathrm{d}t = \theta_\mathrm{d}(t) - \omega_n \int [\theta_0(t) - \theta_1(t)]\,\mathrm{d}t. \tag{9}$$

From (9), it is observed that the output angle of the actuator is equal to the reference input when a vibration transmission does not exist in the system, i.e., τ_0 is equal to zero. With respect to the rest-to-rest maneuvers, the vibration of the system tends to be zero under the action of active damping. Thus, the wave-based control can ensure that the actuator reaches the steady-state desired position and absorbs the vibration energy within the system.

3.2 Hybrid control strategy for vibration suppression of the compounded system

After capturing the large flexible spacecraft, the space robot "grasps" the large flexible spacecraft for on-orbit operations such as target berthing. Two control objectives exist for this maneuver, namely the movement of the space manipulator to a desired position and the vibration suppression of flexible components. The joints of a space manipulator have flexible components, such as harmonic reducers, and thus the entire compounded system can be treated as a lumped flexible system that is connected by torsion springs. With respect to the aim of this compounded system, a hybrid control strategy combining wave-based control and PD control is adopted for vibration suppression during the rest-to-rest maneuvers on-orbit. The control block diagram mainly includes trajectory planning, wave-based control, joint PD control, and the system dynamics model as shown in Figure 7.

Trajectory planning module generates the trajectory of a space manipulator joint based on on-orbit operation tasks. The wave-based control module processes the desired value Θ_d obtained from the trajectory planning module based on the principle of wave-based control as described in Subsection 3.1. The superposition of the launch displacement Θ_a and return displacement Θ_b is used as the actual input value of the manipulator joints. Additionally, Θ_a and Θ_b are calculated based on (6) and (7), respectively.

The output displacements of the motor and manipulator joint torque are used as the feedback information to calculate the return displacement $\varTheta_b$.

$$\varTheta_w = \varTheta_a + \varTheta_b = \frac{1}{2}\varTheta_{\rm d} + \frac{1}{2}\left(\varTheta - \frac{1}{Z}\int \tau_m {\rm d}t\right), \tag{10}$$

where $\varTheta_w$ denotes the actual input of the manipulator joint that is obtained by shaping the desired input by using the wave-based controller. The control torque of the motor of manipulator joint is then obtained by the PD controller as follows:

$$\tau_s = K_{\rm p}(\varTheta_w - \varTheta) + K_{\rm d}(\dot{\varTheta}_w - \dot{\varTheta}), \tag{11}$$

where $K_{\rm p}$ and $K_{\rm d}$ denote the proportional and derivative control coefficient matrices, respectively. The joint torque τ_m in the current state is calculated by (3). By substituting τ_s and τ_m into the second formula of the dynamic (4), the output displacement, denoted as $\varTheta$, of the joint motor of next moment is obtained. According to (3), using the new value of $\varTheta$ updates the joint torque τ_m, and substituting τ_m into the first formula of dynamic (4) obtains the system state variables at the next moment.

Substituting (10) into (11), the following equation is obtained:

$$\tau_s = \frac{1}{2}\left(K_{\rm p}e + K_{\rm d}\dot{e}\right) - \frac{1}{2Z}\left(K_{\rm p}\int \tau_m {\rm d}t + K_{\rm d}\tau_m\right), \tag{12}$$

where $e = \varTheta_{\rm d} - \varTheta$. As indicated in a study by (12), the control torque of the manipulator joint consists of two parts. The first part is related to PD control law and guarantees that the manipulator joint motion tracks a desired trajectory. The second part is related to the joint torque and ensures that the vibration energy of the system is restrained or absorbed. With respect to the rest-to-rest maneuvers, the vibration of the system also tends to zero under the action of active damping. The manipulator joints attain the desired steady-state position through the PD control. Thus, for the rest-to-rest maneuvers, the final steady states of the system correspond to $\lim_{t\to\infty} e \to 0$ and $\lim_{t\to\infty}(\theta - q) \to 0$.

3.3 Stability analysis

With respect to the dynamic (12), the following properties hold:

Property 1. The inertial matrix $H(y)$ is a symmetric positive definite matrix that verifies as follows:

$$\lambda_m \leqslant \|H(y)\| \leqslant \lambda_M, \tag{13}$$

In (13), λ_m and λ_M denote the minimal and maximal eigenvalues of H.

Property 2. The matrix $\frac{1}{2}\dot{H}(y) - C(y, \dot{y})$ is skew symmetric, and thus the following expression holds

$$\dot{y}^{\rm T}\left(\frac{1}{2}\dot{H}(y) - C(y, \dot{y})\right)\dot{y} = 0. \tag{14}$$

The following relationships are defined:

$$\begin{cases} \varDelta = \varTheta - q, \\ \tilde{\varTheta} = \varTheta_{\rm d} - \varTheta - \omega_n \int \varDelta {\rm d}t, \\ \tilde{q} = q_{\rm d} - q - \omega_n \int \varDelta {\rm d}t. \end{cases} \tag{15}$$

The control law (12) can be rewritten as follows:

$$\tau_s = \frac{1}{2}K_{\rm p}\left(e - \omega_n \int \Delta {\rm d}t\right) + \frac{1}{2}K_{\rm d}\left(\dot{e} - \omega_n \Delta\right). \tag{16}$$

By setting all derivatives in (4) to zero for the desired equilibrium point and including $\varphi_{\rm d} = 0$, the desired motor position is equal to the desired link position as follows:

$$\Theta_{\rm d} = q_{\rm d}. \tag{17}$$

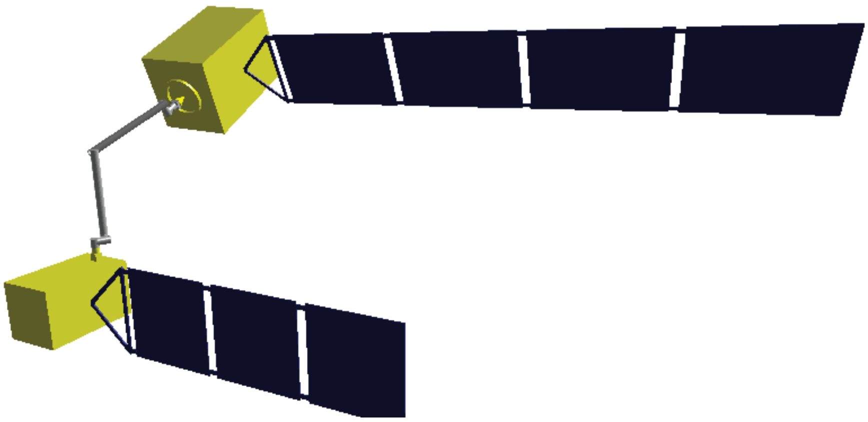

Figure 8 (Color online) The compounded system.

In order to prove the stability of the controller, the following Lyapunov function candidate is considered:

$$V = \frac{1}{2}\dot{\tilde{\Theta}}^{\mathrm{T}} J \dot{\tilde{\Theta}} + \frac{1}{2}\dot{y}^{\mathrm{T}} H \dot{y} + \frac{1}{2}\left(\tilde{\Theta} - \tilde{q}\right)^{\mathrm{T}} K_J \left(\tilde{\Theta} - \tilde{q}\right) + \frac{1}{2}\varphi^{\mathrm{T}} K_{\varphi}\varphi + \frac{1}{4}\tilde{\Theta}^{\mathrm{T}} K_{\mathrm{p}} \tilde{\Theta} + \frac{1}{2}(\omega_n \Delta)^{\mathrm{T}} J (\omega_n \Delta). \quad (18)$$

Evidently V is positive definite. The derivative of the Lyapunov function V is as follows:

$$\dot{V} = \dot{\tilde{\Theta}}^{\mathrm{T}} J \ddot{\tilde{\Theta}} + \dot{y}^{\mathrm{T}} H \ddot{y} + \frac{1}{2}\dot{y}^{\mathrm{T}} \dot{H} \dot{y} + \left(\dot{\tilde{\Theta}} - \dot{\tilde{q}}\right)^{\mathrm{T}} K_J \left(\tilde{\Theta} - \tilde{q}\right) + \dot{\varphi}^{\mathrm{T}} K_{\varphi}\varphi + \frac{1}{2}\dot{\tilde{\Theta}}^{\mathrm{T}} K_{\mathrm{p}} \tilde{\Theta} + (\omega_n \Delta)^{\mathrm{T}} J \left(\omega_n \dot{\Delta}\right), \quad (19)$$

Substituting (4), (14)–(17) into (19), results in

$$\dot{V} = -\frac{1}{2}\left(\dot{\Theta} + \omega_n \Delta\right)^{\mathrm{T}} K_{\mathrm{d}} \left(\dot{\Theta} + \omega_n \Delta\right) - (\omega_n \Delta)^{\mathrm{T}} K_J \Delta + \left(\dot{\Theta} + 2\omega_n \Delta\right)^{\mathrm{T}} J \omega_n \dot{\Delta}, \quad (20)$$

It is assumed that $\dot{\Delta} = \varepsilon\dot{\Theta}$. By substituting $\dot{\Delta} = \varepsilon\dot{\Theta}$ and $\omega_n = \frac{1}{\lambda}\sqrt{\frac{k_J}{J}}$ into (20), the following relationship is obtained:

$$\dot{V} = -\frac{1}{2}\left(\dot{\Theta} + \omega_n \Delta\right)^{\mathrm{T}} (K_{\mathrm{d}} - 2J\omega_n\varepsilon) \left(\dot{\Theta} + \omega_n \Delta\right) - \Delta^{\mathrm{T}} \left[\omega_n^{\mathrm{T}} K_J \left(1 + \frac{1}{\lambda^2}\varepsilon\right)\right] \Delta. \quad (21)$$

Sufficiently high values of K_{d} and λ can be selected to guarantee $K_{\mathrm{d}} - 2J\omega_n\varepsilon > 0$ and $1 + \frac{1}{\lambda^2}\varepsilon > 0$. Additionally, ω_n and K_J are consistently greater than zero. Thus, it is guaranteed that $\dot{V}$ is negative semi-definite. This implies that it is not possible for the energy along the system trajectories to increase. The controlled system is energy dissipative. The proposed control law (12) can guarantee the stability of the closed-loop control system.

4 Simulation study

4.1 A 3D simulation model and the model parameters

The compounded system (shown in Figure 8) used for the simulation is composed of a space robot with a central rigid body, a flexible solar paddle and a 7-DOF serial manipulator, and a target spacecraft with a central rigid body and a flexible solar paddle.

The centroid frames are used as the body-fixed frames of the system bodies. Figure 9 shows the coordinate systems for the robot base and its solar wing. Frames $O_1x_1y_1z_1$ and $O_{10}x_{10}y_{10}z_{10}$ denote the centroid frame of the robot base B_1 and appendage B_{10}, respectively. Both their origins are located in the center of mass (CM). The coordinate systems of the target spacecraft are shown in Figure 10, where, $O_9x_9y_9z_9$ and $O_{11}x_{11}y_{11}z_{11}$ respectively are the centroid frames of target base B_9 and appendage B_{11}. The body-fixed frames of the space manipulator are defined as Figure 11 (when all the joint angles

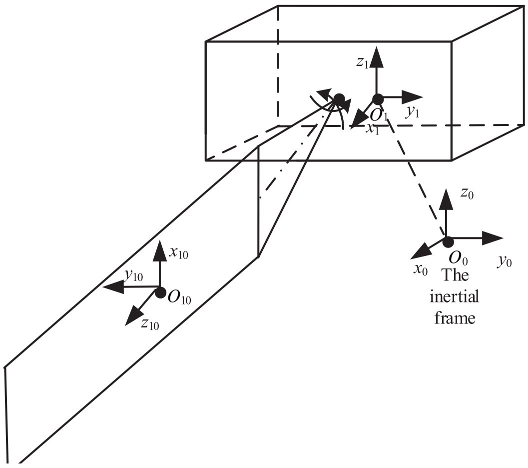

Figure 9 The coordinate system of the robot base and its solar wing.

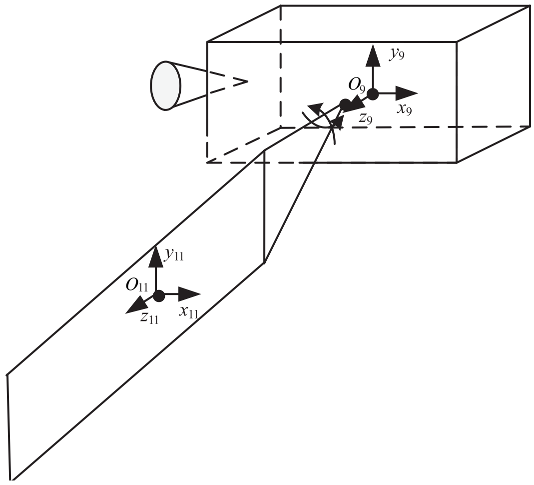

Figure 10 The coordinate system of the target base and its solar wing.

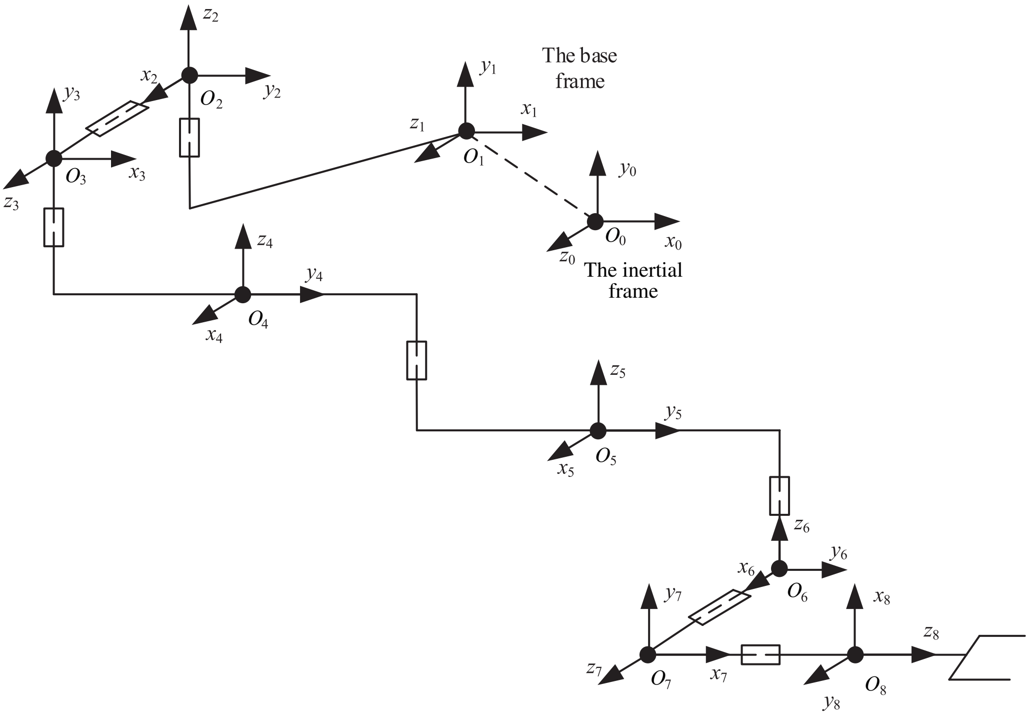

Figure 11 The coordinate system of the space manipulator.

correspond to zero). The origins are located in the centroid of each link of the manipulator. The z-axes of the frames correspond to the rotation directions of the corresponding joints.

The solar wing of the space robot (i.e., body B_{10}) is installed at [0 m, 0 m, 0.75 m] with respect to the centroid frame of B_1. The solar wing of the target (i.e., body B_{11}) is installed at [0 m, 0 m, 1.05 m] with respect to the centroid frame of B_9. With respect to B_{10}, the virtual torsion spring stiffness of the bending vibration and torsional vibration correspond to 2000 Nm/rad and 3000 Nm/rad, respectively. The bending frequency and torsional frequency of the appendage B_{10} are 0.3013 Hz and 1.949 Hz, respectively. With respect to B_{11}, the virtual torsion spring stiffness of bending vibration and torsional vibration are 1000 Nm/rad and 1500 Nm/rad, respectively. The bending frequency and torsional frequency of the appendage B_{11} are 0.091 Hz and 1.165 Hz, respectively. The stiffness of each

Table 1 The mass properties of the rigid bodies

Parameter	B_1	B_2	B_3	B_4	B_5	B_6	B_7	B_8	B_9	B_{10}	B_{11}
Mass (kg)	1500	15	15	30	30	15	15	30	3000	30	45
	0	0	0.15	0	0	0	0	0	1.8	–	–
a_i (m)	0	0	0	1.15	1.15	0	0	0	0	–	–
	0	0.15	0	−0.15	−0.15	−0.15	0.15	0.25	0	–	–
	0.9	0.15	0	0	0	0.15	0.15	0	–	0	0
b_i (m)	1.1	0	−0.15	1.15	1.15	0	0	0	–	0	0
	0	0	0	−0.15	−0.15	0	0	0.44	–	4.5	7
	100	1	1	2	2	1	1	2	200	558	3054
I ($\mathrm{kg}\cdot\mathrm{m}^2$)	100	1	1	2	2	1	1	2	200	537	3025
	100	1	1	2	2	1	1	2	200	20	28

manipulator joint corresponds to 10000 Nm/rad. The mass properties of the compounded system are listed in Table 1. All the inertias of the joint rotor correspond to 0.01 $\mathrm{kg}\cdot\mathrm{m}^2$.

4.2 Vibration suppression for target berthing mission

Immediately following the captured of the target (i.e., the pre-capture and contact/impact stages are finished), the space manipulator is in a non-ideal configuration for the next on-orbital servicing tasks. Thus, it is necessary to move the target to the normal configuration. This process is termed as target berthing, and the normal configuration is termed as the berthing configuration.

It is assumed that the initial angle of the virtual torsion spring of bending vibration and torsional vibration correspond to 5° and 1°, respectively, and the capture configuration and the berthing configuration are as follows:

$$\Theta_0 = \begin{bmatrix} 60^\circ & 90^\circ & 0^\circ & -60^\circ & 0^\circ & -30^\circ & 110^\circ \end{bmatrix}, \tag{22}$$

$$\Theta_f = \begin{bmatrix} 90^\circ & 90^\circ & -80^\circ & -100^\circ & 90^\circ & 0^\circ & 90^\circ \end{bmatrix}. \tag{23}$$

The 3D states corresponding to (22) and (23) are shown in Figures 8 and 12. They are supplied by a closed-loop simulation system developed in [16]. The 5th polynomial function is used to plan the joint trajectory. The total simulation time length corresponds to 80 s, and the time for joint trajectory planning is 15 s. Hence, the manipulator moves to the berthing configuration at 15 s.

The simulation results are shown in Figures 13–17. Figure 13 shows the vibration curve of the flexible wing. Additionally, φ_1 and φ_2 represent the torsional deformation and bending deformation of appendage B_{10}, respectively. Furthermore, φ_3 and φ_4 represent the torsional deformation and bending deformation of appendage B_{11}, respectively. As shown in Figure 13, the use of the PD control does not result in a significant attenuation in the residual vibration. However, the vibration is evidently reduced when the hybrid control method is used, and the value of the torsional deformation quickly approaches zero after 20 s. The magnitude of the vibration of the flexible appendage obtained by the hybrid control method is significantly lower than that obtained by the PD controller. With respect to the PD control, the final values of the bending deformation of B_2 and B_{10} correspond to 0.127° and 6.86°, respectively. However, with respect to the hybrid control, the final values of the bending deformation of B_2 and B_{10} only correspond to 0.0073° and 0.295°, respectively.

Figure 14 shows the joint torques generated by joint deformation. According to (3), the joint torque is proportional to the joint deformation, and the proportional coefficient corresponds to the joint stiffness. As shown in Figure 14, the values of the joint torque under the PD control exceed those under hybrid control. A large residual torque fluctuation is observed in joint 1, joint 2, joint 6, and joint 7 after 15 s. This is because the vibration of these joints interacts with the vibration of the flexible appendages and transmits the vibration motion between themselves. Figure 13 is compared with Figure 14, and it is observed that the vibration of joints and the vibration of appendages almost exhibit synchronous attenuation.

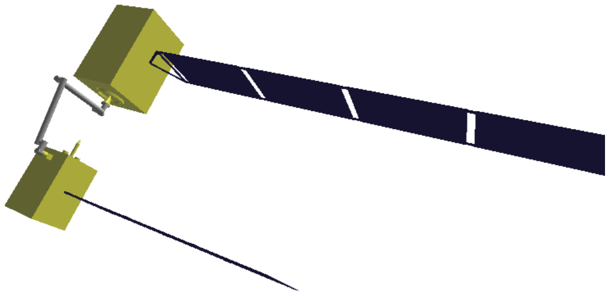

Figure 12 (Color online) The berthing configuration of the compounded system.

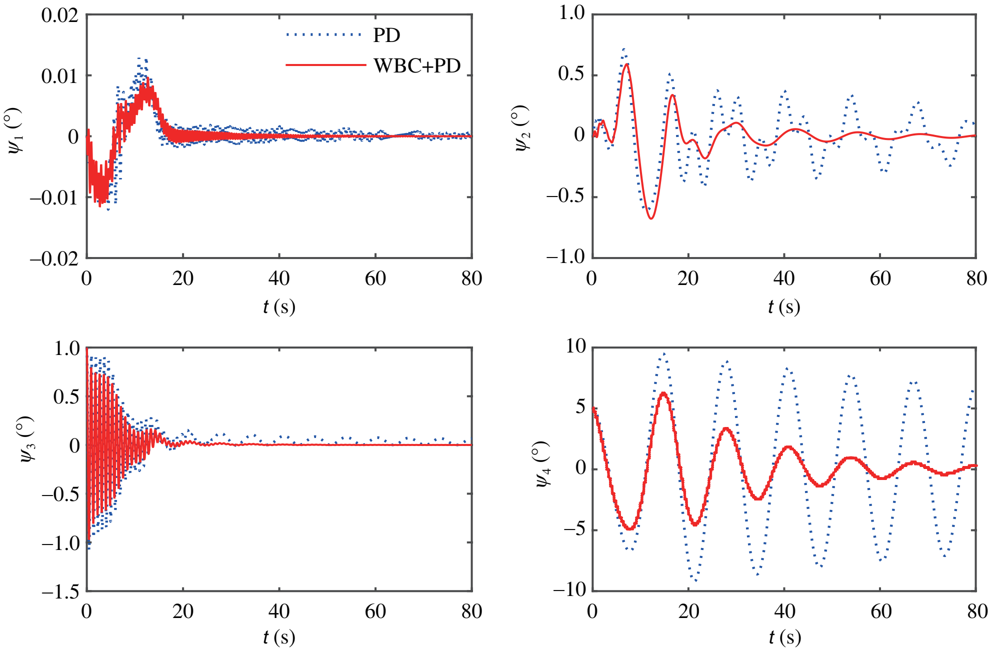

Figure 13 (Color online) The curves of the deformation angle of the torsion spring of the appendages.

Figures 15 and 16 show the motor angles and joint angles, respectively. As shown in the fore-mentioned two graphs, the motor angles as well as the joint angles can track the desired trajectories. There is a delay in tracking the desired trajectory of the joint under the hybrid control. However, it can be controlled within a reasonable extent, and this is not important for the rest-to-rest movement. The final position deviations of all joints are within 0.5° with respect to the hybrid control. The joints have larger flexibility, and the hybrid control provides a higher level of guarantee that the joint tracks the desired trajectory.

The position and orientation of the space robot's base are shown in Figure 17. The final position and orientation of the robot base are essentially the same under both the control methods. The attitude and the centroid position of the base vary from $[0^\circ, 0^\circ, 0^\circ]^{\mathrm{T}}$ to $[8.6^\circ, -4.25^\circ, -53^\circ]^{\mathrm{T}}$ and from $[0\ \mathrm{m}, 0\ \mathrm{m}, 0\ \mathrm{m}]^{\mathrm{T}}$ to $[1.01\ \mathrm{m}, 0.94\ \mathrm{m}, 0.175\ \mathrm{m}]^{\mathrm{T}}$, respectively. Nevertheless, α, β attitude angles and the displacement in the x direction exhibit higher vibrations under the PD control.

As shown in Figures 14 and 17, it is observed that the position and orientation of the base in certain specific directions and certain specific manipulator joints exhibit large oscillations. The bending vibration of the windsurfing causes a large displacement oscillation of the base in a direction perpendicular to the solar paddle plane and a large attitude oscillation of the base in a direction parallel to the solar paddle plane. The vibration energy of the solar paddle is then further transmitted to the corresponding manipulator joints via the satellite base. Finally, the vibration energy of the attachment is measured and actively absorbed at the manipulator joints. Therefore, it is only necessary to perform information measurement and control at the manipulator joints by using the wave-based method. It is very easy

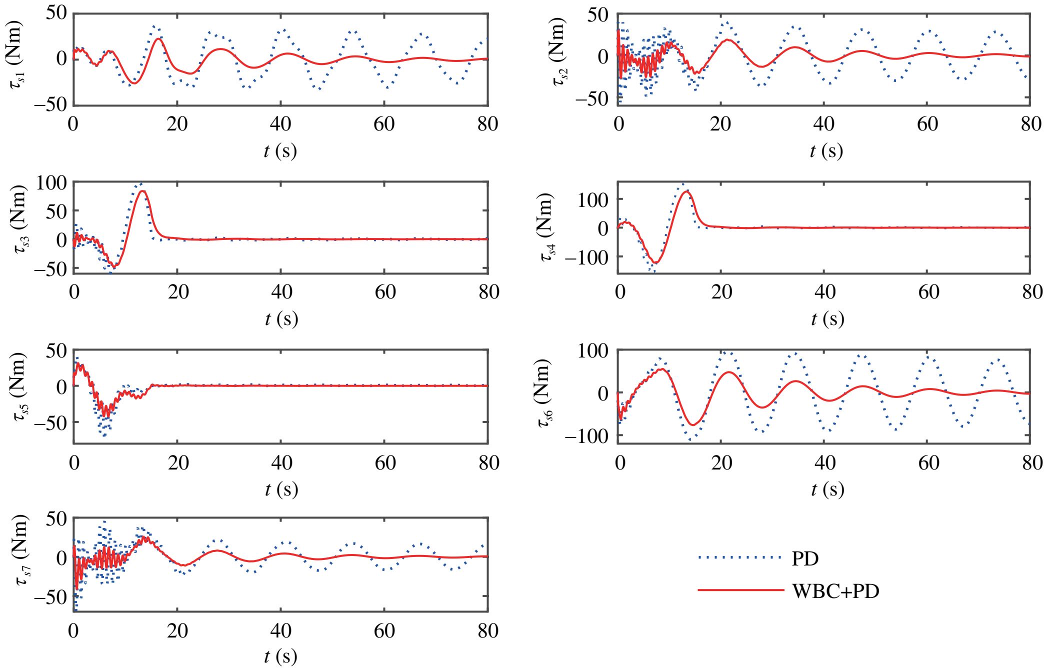

Figure 14 (Color online) The curves of the joint torques.

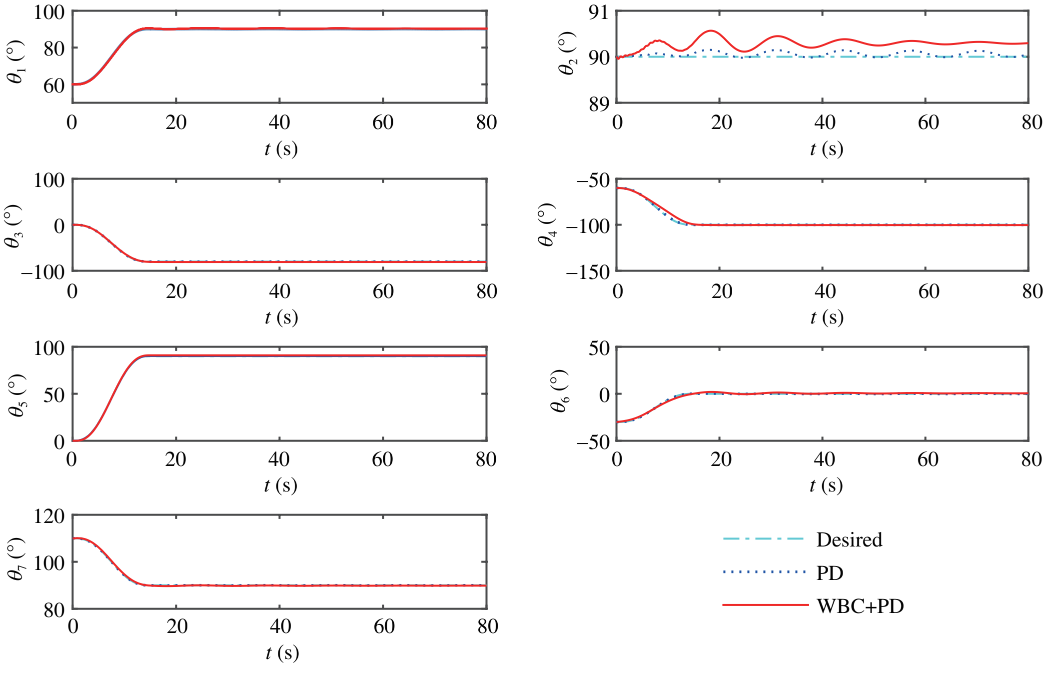

Figure 15 (Color online) The curves of the motor angles.

to implement this method in the vibration control of non-cooperative large flexible spacecrafts and a significant control effect is observed.

5 Conclusion

The application of a space robot with flexible appendages in space involves structure flexibility that can easily cause vibration during the orbit and/or attitude maneuver of the base and the operation of the manipulator. In the present study, the compounded system was treated as a lumped flexible

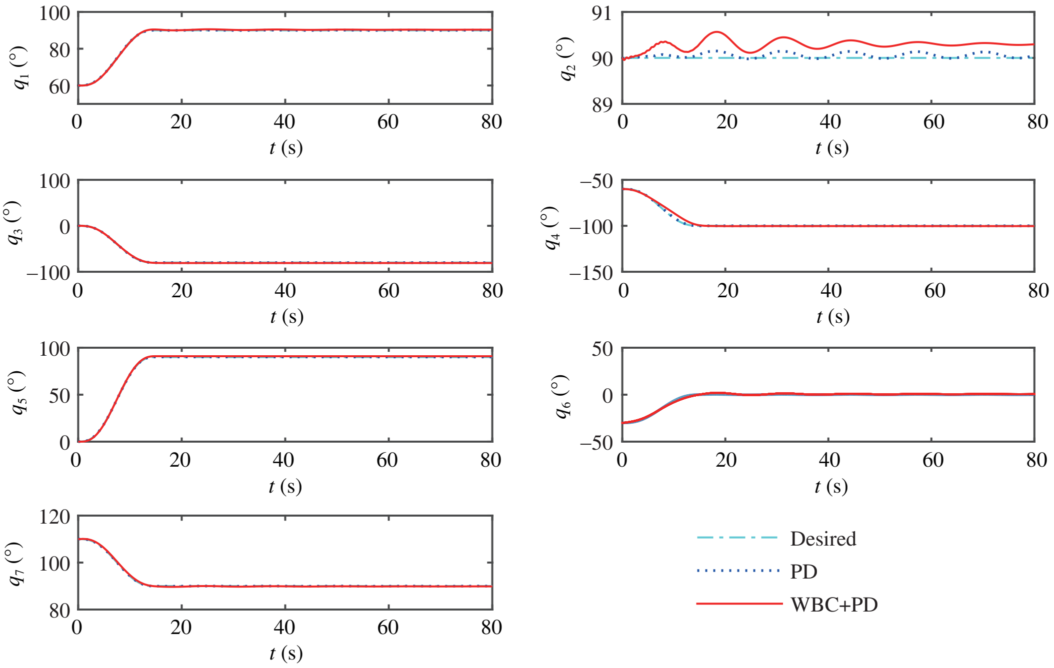

Figure 16 (Color online) The curves of the joint angles.

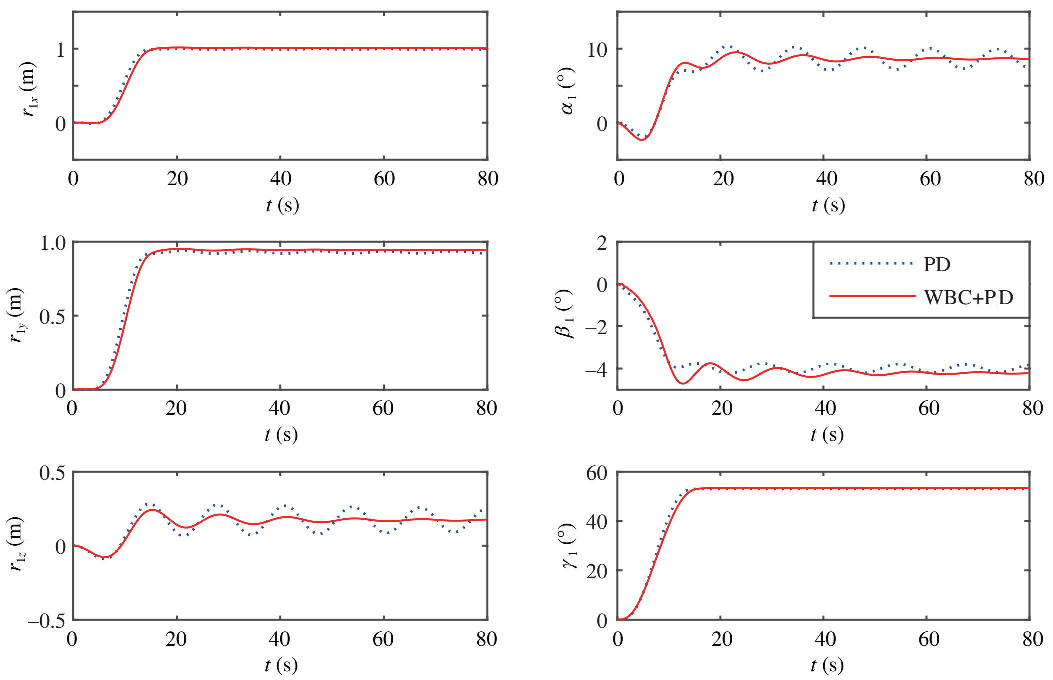

Figure 17 (Color online) The position and orientation of the space robot base.

system based on the flexible joints and flexible appendages. The vibration control of the compounded system was performed by combining the wave-based method and PD control. First, the rigid-flexible coupling dynamics of the compounded system with flexible appendages and flexible manipulator joints were derived. This was followed by proposing a hybrid control method to control the motion of the manipulator and suppress the vibration of large flexible components. Finally, a simulation study was performed to verify the effectiveness of the proposed method. The results indicated that with respect to the rest-to-rest operation tasks, the effectiveness of the wave-based control method was considerably higher than that of the PD control. A future study will involve the integration of the wave-based control method into a servo motor and performing experimental research through an air floating platform.

Acknowledgements This work was supported by National Natural Science Foundation of China (Grant No. 61573116), Natural Science Foundation of Guangdong Province (Grant Nos. 2014A030310318, 2015A030313881) and Basic Research Program of Shenzhen (Grant Nos. JCYJ20140417172417095, JCYJ20160427183553203).

Conflict of interest The authors declare that they have no conflict of interest.

References

1 Shan M H, Guo J, Gill E. Review and comparison of active space debris capturing and removal methods. Prog Aerosp Sci, 2016, 80: 18–32

2 Flores-Abad A, Ma O, Pham K, et al. A review of space robotics technologies for on-orbit servicing. Prog Aerosp Sci, 2014, 68: 1–12

3 Sellmaier F, Boge T, Spurmann J, et al. On-orbit servicing missions: challenges and solutions for spacecraft operations. In: Proceedings of AIAA SpaceOps Conference, Huntsville, 2010. 25–30

4 Stoll E, Letschnik J, Walter U, et al. A review of space robotics technologies for on-orbit servicing. IEEE Robot Autom Mag, 2009, 16: 29–33

5 Nagashio T, Kida T, Ohtani T, et al. Design and implementation of robust symmetric attitude controller for ETS-VIII spacecraft. Control Eng Pract, 2010, 18: 1440–1451

6 Sylla M, Asseke B. Dynamics of a rotating flexible and symmetric spacecraft using impedance matrix in terms of the flexible appendages cantilever modes. Multibody Syst Dyn, 2008, 19: 345–364

7 Gasbarri P, Pisculli A. Dynamic/control interactions between flexible orbiting space-robot during grasping, docking and post-docking manoeuvres. Acta Astronaut, 2015, 110: 225–238

8 Yu Z W, Liu X F, Cai G P. Dynamics modeling and control of a 6-DOF space robot with flexible panels for capturing a free floating target. Acta Astronaut, 2016, 128: 560–572

9 Zarafshan P, Moosavian S A A, Papadopoulos E G. Adaptive hybrid suppression control of space free-flying robots with flexible appendages. Robotica, 2016, 34: 1464–1485

10 Hirano D, Fujii Y, Abiko S, et al. Vibration suppression control of a space robot with flexible appendage based on simple dynamic model. In: Proceedings of the IEEE International Conference on Intelligent Robots and Systems, Tokyo, 2013. 789–794

11 Hirano D, Fujii Y, Abiko S, et al. Simultaneous control for end-point motion and vibration suppression of a space robot based on simple dynamic model. In: Proceedings of the IEEE International Conference on Robotics and Automation, Hong Kong, 2014. 6631–6637

12 Kojima H, Ieda S, Kasai S. Frequency-tuning input-shaped manifold-based switching control for underactuated space robot equipped with flexible appendages. Acta Astronaut, 2014, 101: 42–54

13 Kasai S, Kojima H. Input-shaped link motion control of planar space robot equipped with flexible appendage. Trans Jpn Soc Aeronaut Space Sci, 2012, 55: 205–213

14 Azadi M, Eghtesad M, Fazelzadeh S A, et al. Dynamics and control of a smart flexible satellite moving in an orbit. Multibody Syst Dyn, 2015, 35: 1–23

15 Azadi M, Fazelzadeh S A, Eghtesad M, et al. Vibration suppression and adaptive-robust control of a smart flexible satellite with three axes maneuvering. Acta Astronaut, 2011, 69: 307–322

16 Xu W F, Meng D S, Chen Y Q, et al. Dynamics modeling and analysis of a flexible-base space robot for capturing large flexible spacecraft. Multibody Syst Dyn, 2014, 32: 357–401

17 O'Connor W J, Lang D. Position control of flexible robot arms using mechanical waves. J Dyn Syst Meas Control, 1998, 120: 334–339

18 O'Connor W J. Wave-based analysis and control of lump-modeled flexible robots. IEEE Trans Robot, 2007, 23: 342–352

19 Cleary S, O'Connor W J. Control of space debris using an elastic tether and wave-based control. J Guid Control Dynam, 2016, 39: 1392–1406

20 Marek O. Servo control using wave-based method. In: Advances in Mechanisms Design. Berlin: Springer, 2012. 531–536

21 Malzahn J, Bertram T. On the equivalence of direct strain feedback and lumped parameter wave echo control for oscillation damping of elastic-link arms. IEEE Robot Autom Lett, 2016, 1: 447–454

22 Saigo M, Tanaka N. Torsional vibration suppression by wave absorption controller. J Sound Vib, 2006, 295: 317–330

23 Spong M W. Modeling and control of elastic joint robots. J Dyn Syst Meas Cont, 1987, 109: 310–318

24 Bonollo P. Wave-based control of multi-DoF flexible models for aerospace launchers. Dissertation for Master Degree. Veneto Padua: Universit degli Studi di Padova, 2016

25 O'Connor W J, Habibi H. Wave-based control of under-actuated flexible structures with strong external disturbing forces. Int J Control, 2015, 88: 1818–1829